Catalysis Letters Vol. 110, Nos. 3–4, September 2006 (© 2006)
DOI: 10.1007/s10562-006-0111-1

Remarks on the passivation of reduced Cu-, Ni-, Fe-, Co-based catalysts

Florian Huber,[a] Zhixin Yu,[a] Sara Lögdberg,[b] Magnus Rønning,[a] De Chen,[a] Hilde Venvik,[a,*] and Anders Holmen[a]

[a]*Department of Chemical Engineering, Norwegian University of Science and Technology (NTNU), N-7491 Trondheim, Norway*
[b]*Department of Chemical Engineering and Technology, Royal Institute of Technology (KTH), SE-100 44 Stockholm, Sweden*

Received 2 April 2006; accepted 6 April 2006

Catalysts containing metals such as Cu, Ni, Fe, Co in their reduced state are often subjected to passivation procedures prior to characterization. Passivation with N_2O or O_2 to create a protective oxide layer also results in a certain degree of sub-surface oxidation. The heat released during oxidation is a critical parameter. The extent of bulk oxidation depends on the type of oxidant as well as on the size of the metal particles, as shown for copper catalysts. The final, meta-stable passivation layer requires a certain thickness to sustain exposure to ambient atmosphere. The encapsulation of metal particles in carbon is an efficient method for preserving the metallic state, as demonstrated for metallic nickel and iron with carbon nanofibers. The use of passivated samples for characterization of the active, i.e., reduced, catalyst has limited value.

KEY WORDS: passivation; encapsulation; reduced metals; Cu; Ni; Fe; Co; surface and bulk oxidation; O_2; N_2O; CO; CO_2; carbon.

1. Introduction

Catalysts comprising the transition metals Cu, Ni, Fe and Co are widely applied in heterogeneous catalysis. In most cases, the active catalysts contain these transition metals in their reduced, i.e., metallic, state rather than as an oxide. Under oxidizing conditions, such as in air, the metallic state of Cu, Ni, Fe and Co is unstable. Depending on the conditions, the metals will be partly or completely re-oxidized to their stable oxides: $Cu \rightarrow Cu_2O/CuO$ [1], $Ni \rightarrow NiO$, $Fe \rightarrow Fe_3O_4/Fe_2O_3$ [2], $Co \rightarrow CoO/Co_3O_4$ [3,4].

In order to characterize material properties relevant to the catalytic performance of the catalyst, the metal particles should be studied in the activated state, preferably during the catalytic reaction, i.e., *in situ*. Several *in situ* studies have shown metal catalysts to undergo dynamic structural changes depending on the reaction atmosphere (oxidizing or reducing) [5–9]. However, *in situ* characterization can be time-consuming or require equipment not readily available. To be able to characterize reduced metal catalysts, a range of protection methods are applied to retain the reduced state of metal catalysts during characterization or transfer to the characterization chamber:

1. Sealing in a container under reducing/inert atmosphere after reduction [10]
2. Encapsulation of the reduced metal particles
   a. by deposition of polyethylene [11–13] or 1-butene films [14] on the surface, analogous to the protection of bulk metals against corrosion by coating with polymer films
   b. by growing a layer of carbon (such as carbon nanofibers or paraffinic wax) around the reduced metal particles [15–17]
3. Surface passivation of reduced metal particles by controlled re-oxidation to create a thin, protective oxide layer. Further oxidation of the bulk is inhibited by diffusion limitation [18]. A quasi- or meta-stable reduced metal phase is maintained below the protection layer. Oxidant gases that have been applied include:
   a. O_2/air in inert gas [1,18–23]
   b. N_2O in inert gas [9,24–27]
4. Formation of combined carbonaceous and oxidic layers, applying
   a. CO_2/O_2, CO_2/H_2O or $CO_2/H_2O/O_2$, optionally in inert gas [28–31]
   b. $CO/H_2$and O_2/air (consecutive) [32].

Our group has previously reported the successful application of sealed quartz capillaries for preserving activated catalysts [10]. In this study, we evaluate and share our experience with other protection methods, namely O_2 and N_2O passivation, and relate our findings to reports on passivation in the literature. In addition, the encapsulation in carbon nanofibers (CNF) for a range of catalysts used in the ongoing research is reported and proposed as a possible method.

*To whom correspondence should be addressed.
E-mail: Hilde.Venvik@chemeng.ntnu.no

2. Experimental

2.1. Catalyst samples

The copper catalysts are mixed metal oxides derived from hydrotalcite precursors. Cu-350 and Cu-400 contain CuO, ZnO and Al_2O_3 after the final calcination at 350 and 400 °C, respectively, and their hydrotalcite precursors were prepared by coprecipitation. Ce-bC-400 was made from Cu-400 by incipient wetness impregnation of the dried sample with a cerium nitrate solution. Details on preparation, sample notation and catalyst properties can be found elsewhere [33].

The Ni–Fe catalyst is designed for carbon nanofiber (CNF) production and contains both metals in a molar ratio Ni:Fe = 8:2. The catalyst, composed of NiO, Fe oxides (Fe_2O_3 and Fe_3O_4) and Al_2O_3 after calcination, was prepared by coprecipitation to produce a hydrotalcite precursor. The CNF were synthesized by catalytic chemical vapour deposition from $C_2H_4/CO/H_2$ (30/10/10 ml/min) at 600 °C for 1 h. Further details on catalyst preparation and properties have been previously reported [15].

The Fischer–Tropsch (FT) catalyst containing 12 wt% cobalt was prepared by incipient wetness impregnation of silica (PQ corp. CS-2133) with an aqueous solution of $Co(NO_3)_2{\cdot}6H_2O$. The impregnated powder was dried in air at 120 °C for 3 h and calcined at 300 °C for 16 h, increasing the temperature from 120 to 300 °C at a rate of 1 °C/min. Further details on this type of catalyst have been published elsewhere [3,34].

2.2. Characterization

Inductively Coupled Plasma Atomic Emission Spectroscopy (ICP-AES) was used to determine the actual amount of copper in the catalyst samples after calcination. The samples were dissolved in hydrochloric acid prior to this analysis without any visible residues.

Copper dispersion and passivation measurements by means of N_2O decomposition [22,27,35,36] according to the exothermic reaction

$$2Cu + N_2O \rightarrow Cu_2O + N_2 \qquad (1)$$

were performed in a Thermogravimetric Analyser (Perkin Elmer TGA 7) using approx. 50 mg sample and 10 vol% N_2O in argon (reaction temperature: 75 °C, flow rate: 80 ml/min at ambient pressure/temperature, 1 h under N_2O atmosphere until the baseline was stabilized). Temperature-programmed reduction (TPR) using 7 vol% H_2 in argon (260 °C, 2 h, heating rate 2 K/min, flow rate 80 ml/min at ambient pressure/temperature) as well as the estimation of weight loss assigned to adsorbed water and/or surface carbonates of the calcined samples [37], were carried out in the same apparatus. TPR was also carried out with 7 vol% CO in argon over Ce-bC-400, with the reduced catalyst being cooled down in CO/Ar prior to N_2O titration. The weight loss (at 260 °C after 1 h in Ar) was determined prior to reduction (at 260 °C for 2 h) and dispersion measurements. Dispersion calculations based on oxygen chemisorption from N_2O decomposition with a simplified reaction stoichiometry of Cu:O = 2 corresponding to equation (1) were corrected for bulk oxidation of copper according to the method proposed by Sato *et al.* [38].

The passivation of the copper catalysts with O_2 was also performed in the TGA. In a typical experiment, the catalyst sample was dried (260 °C, 1 h, Ar), reduced (260 °C, 2 h, 7 vol% H_2 in Ar) and passivated (ambient temperature, 2 h, 1 vol% oxygen in Ar, 100 ml/min). The exothermic re-oxidation can be written as follows [1,20]:

$$2Cu + {}^1/_2O_2 \rightarrow Cu_2O \qquad (2)$$

Hence, a simplified reaction stoichiometry of Cu:O = 2 is assumed. Pernicone *et al.* [20] have discussed the reaction stoichiometry and the possibility of non-integer stoichiometry. For the erroneous impact of the support (especially reducible metal oxides like ceria or zirconia, and partly ZnO) on the quantification of dispersion and passivation extent, we refer to Bartley *et al.* [27]. Concerning the stability of Cu_2O phases, Palkar *et al.* [39] report that cubic Cu_2O is more stable than monoclinic CuO at small crystallite sizes (< 25 nm). This is related to the increasing ionic character of solids with decreasing particle size and is also dependent on calcination conditions.

XRD spectra for crystallite size estimation and phase identification of the (O_2-passivated) copper catalysts were recorded on Siemens diffractometers D-5000 (monochromatic CuK_α-radiation) and D-5005 (dichromatic $CuK_{\alpha+\beta}$-radiation), respectively. Particle size estimates (d_P) for the reduced-(O_2)passivated copper samples were calculated by X-ray line broadening analysis (XLBA, linewidth at half maximum, B) of the Cu(111) reflection at the Bragg angle P = 21.67° using the Scherrer equation and LaB_6 as a standard for correction of instrumental line broadening (B_e)

$$d_p = \frac{K.\lambda}{\sqrt{B^2 - B_e^2} \cdot \cos(\Theta)} \qquad (3)$$

with λ = 1.5418 Å , the wavelength for CuK_α, and K = 0.89, the Scherrer constant. The value of the constant factor K depends on the definition of B, being set equal to 1.00 when using the integral breadth and 0.89 when using the full width at half maximum [40]. The crystallite size of the reduced-passivated samples reported in table 1 takes into account the thickness of the passivation layer assuming a cubic shape for the copper particles.

The passivation of the Co/SiO_2 catalyst was characterized by XRD using the Siemens D-5005 diffractometer. The sample (1 g) was reduced in flowing hydrogen

Table 1
Chemical composition and physical properties of the copper catalyst samples

Sample	H_2O/CO_2 weight loss[a] (wt%)	Total Cu mass fraction in the samples (–)		Cu dispersion[d] (%)	Cu passivated with N_2O[e] (%)	Cu passivated with O_2[e] (%)	Cu crystallite size (with O_2 passivation) (nm)	
		ICP-AES[b]	TGA-TPR[c]				Cu core with XRD[f]	Core + pass.layer (XRD + TGA)[g]
Cu-350	5.7	0.29	0.28	6.5	10	40	19	23
Cu-400	1.7	0.27	0.26	5.4	7	45	20	25
Ce-bC-400	1.7	0.25	0.25	8.2	11	40	20	24

[a] Thermogravimetric measurements performed in Ar on the calcined samples up to the reduction temperature (260 °C) resulted in a weight loss assigned to adsorbed water and/or surface carbonates.
[b] Normalized mass fractions, i.e., only CuO, ZnO, Al_2O_3 and CeO_2 taken into account, with an estimated detection limit of 0.01–0.03 mg/g. The elementary analysis was performed on as-prepared calcined samples, thus containing water/carbonates adsorbed on the surface.
[c] For better comparison with the ICP-AES results the amount of copper determined by TGA-TPR is normalized with the sample mass before the drying procedure.
[d] Copper dispersion measured by means of selective oxidation via N_2O surface titration of the reduced catalyst samples taking into account copper bulk oxidation [38,42], with percentage values being based on mole fraction.
[e] Normalized with amount of Cu determined by TGA-TPR prior to passivation, with percentage values being based on mole fraction.
[f] Performed on the reduced and passivated samples. The copper crystallite size is estimated using the Scherrer equation for the Cu (111) reflection.
[g] The thickness of the passivation layer is taken into account assuming a cubic particle shape.

at atmospheric pressure and 350 °C for 16 h (heating rate: 5 °C/min up to 70 °C and then 1 °C/min up to 350 °C). According to Storsæter *et al.* [34] and references therein, most of the reducible cobalt oxide is reduced after this procedure. Subsequently, the sample was cooled down to ambient temperature, and the quartz reactor was flushed with N_2 5.0 for 2 h. The consecutive passivation was carried out in either of two ways: In one experiment, a gas mixture of 0.5 vol% of O_2 in nitrogen was used (first, 1 h at 50 ml/min and then 1 h at 140 ml/min). In a second experiment, 5 vol% of N_2O in nitrogen was applied (2 h at 140 ml/min). The XRD analysis was started within 2 h after passivation.

Transmission X-ray absorption spectroscopy (XAS) data were recorded for calcined, reduced-O_2-passivated and CNF-encapsulated Ni–Fe samples at the Swiss-Norwegian Beamline (SNBL) at the European Synchrotron Radiation Facility (ESRF) in France. Spectra were obtained at the Fe K-edge (7.112 keV) and Ni K-edge (8.333 keV) using a channel-cut Si(111) monochromator. Higher order harmonics were rejected by means of a chromium-coated mirror aligned with respect to the beam to give a cut-off energy of approximately 15 keV. The software package *WINXAS* v3.1 [41] was used for XANES analysis (X-ray absorption near edge structure) to obtain qualitative and quantitative information on Ni/Fe oxide and metallic phases. The XAS data were calibrated, pre-edge background subtracted (linear fit) and normalized. XAS spectra were collected both for the calcined material, in the reduced-passivated state and after use in CNF production. The passivation was conducted with about 1 vol% of O_2 in nitrogen. Ni and Fe metal foils, NiO, α-Fe_2O_3 and Fe_3O_4 were used as reference materials. The phase composition of the catalyst samples under study was determined by linear combination of the reference XANES profiles applying a least-square fitting procedure in WINXAS.

3. Results

3.1. Copper catalysts

A representative experimental curve from TGA measurements of the copper-containing samples is shown in figure 1. Initially, water and/or carbonate species adsorbed on the surface [37] are removed by increasing the temperature to the final reduction temperature under Ar atmosphere. In this way, the weight change resulting from desorption of adsorbed species does not interfere with the weight change caused by the subsequent reduction. CuO is reduced to metallic copper and oxygen is released as water molecules during TPR, decreasing the sample weight thereby. After reduction

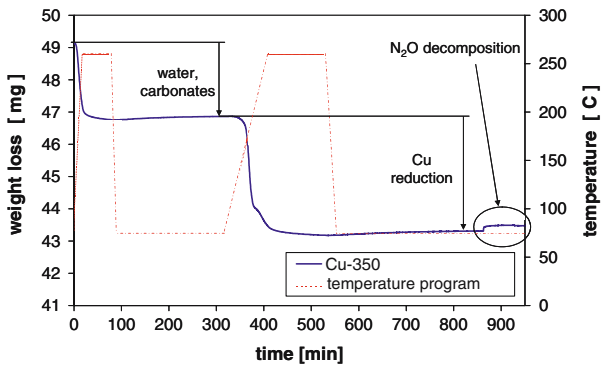

Figure 1. A typical TGA experimental curve, obtained over Cu-350, including removal of water/carbonate species adsorbed on the surface, TPR of Cu and N_2O decomposition for determination of Cu dispersion and passivation.

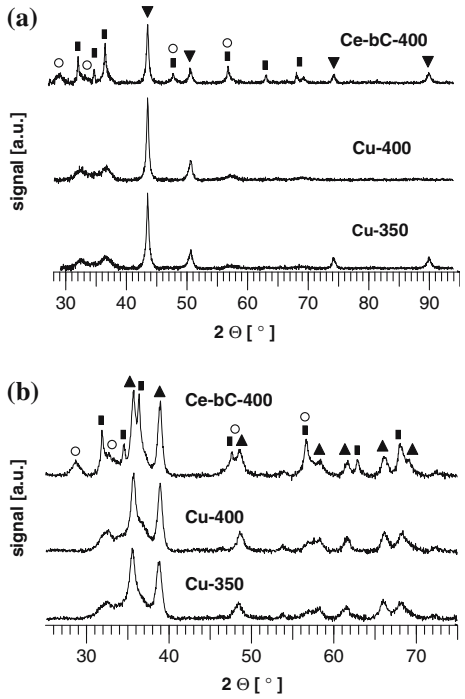

Figure 2. XRD spectra of (a) reduced-(O_2)passivated (D-5000 diffractometer and (b) calcined (D-5005 diffractometer) Cu catalysts. The symbols refer to different crystalline phases: ■ = ZnO, ▲ = CuO, ▼ = Cu, ○ = CeO_2.

and flushing with Ar, N_2O decomposition was carried out to re-oxidize the copper atoms in or close to the surface. By plotting oxygen uptake versus time and scaling the abscissa with the square root of time, surface and bulk oxidation contributions can be separated. Since bulk oxidation is diffusion limited, it will appear as a linear segment in such a diagram. Further details about this approach can be found elsewhere [38,42].

Weight losses caused both by adsorbates and copper reduction for the three copper samples are given in table 1. The copper content as determined by TGA is in good agreement with the ICP-AES results. The copper dispersion of the samples varies between 5 and 8% assuming the $Cu/N_2O = 2$ stoichiometry according to equation (1). The oxygen uptake during N_2O decomposition is correspondingly 7–11%. This indicates that the passivation layer is relatively thin and that the re-oxidation of copper does not reach far into the bulk. In contrast, Cu passivation with O_2 results in a considerably thicker passivation layer, extending to about 40% of the Cu atoms.

The crystallite size of the Cu core embedded in the oxide layer is estimated from XRD spectra recorded for reduced-(O_2)passivated samples (figure 2a). XRD spectra of calcined samples before reduction/passivation are included for comparison (figure 2b). For all three catalyst samples, the size of the Cu core (d_C) is estimated to about 20 nm (table 1). Using a cubic model the average size of the copper particles (d_P), including core and passivation layer, can be estimated by the following equation:

$$d_p = \sqrt{[3]}\frac{1}{(1 - x_p)} \cdot d_C \qquad (4)$$

with x_p being the fraction of the passivated Cu atoms. According to this estimation, the thickness of the oxide layer lies in the range of a few nanometers (table 1), which is in agreement with literature ([20] and references therein). The structural model applied does not, however, take into account possible structural changes during passivation. Several studies have shown that both surface structure as well as particle shape may change (dynamically) upon changes in the gas phase conditions [5–9]. Despite the significant degree of re-oxidation, the oxide layer does not appear in the XRD spectra (figure 2a). The passivation layer is only a few nanometers thick and will therefore appear amorphous to XRD [5,43]. Thus, from XRD alone, the passivation layer appears insignificant. Kvande *et al.* [44] identified a crystalline Cu_2O phase in addition to metallic copper by XRD after passivation of a reduced Cu/CNF catalyst in O_2/He, indicating a significant degree of bulk oxidation.

Pernicone *et al.* [20] report the passivation of a copper-containing catalyst with 60% of the Cu atoms being re-oxidized. This copper catalyst contained smaller copper particles (Cu core: 10.2 nm, with passivation layer: 13.8 nm) than the samples in table 1. If we assume that the passivation layer must reach a certain thickness in order to protect the bulk against further oxidation, the fraction of re-oxidized metal atoms should increase with decreasing particle diameter (equation 4). This trend was also observed within our passivation studies. Another Cu–Zn–Al mixed oxide catalyst, prepared by coprecipitation under different conditions but with a similar composition as the copper catalysts described in Chapter 2.1, showed a passivation degree of about 58% (with oxygen). The size of the copper core was estimated to 10.6 nm, and the particle size, including the passivation layer, to 14.2 nm, in good agreement with the results obtained by Pernicone *et al.*

Figure 3 shows the normalized weight increase of CebC-400 during N_2O titration as a function of the square root of time, based on the total weight loss upon reduction. The pre-reduction was carried out with H_2/Ar and CO/Ar. In both cases, the reduced catalyst was cooled down in the reduction gas prior to N_2O titration. The sample pre-treated with CO/Ar exhibits a slower oxidation kinetics and a lower total oxygen uptake than the sample pre-treated with H_2/Ar. The dispersions determined from the dispersion-square root of time plot correspond to approx. 8.2 and 6.2% for pre-reduction with H_2 and CO, respectively. We assume that carbonaceous species on the surface of the reduced Cu particles slow down and confine the re-oxidation of metallic Cu in the case of pre-reduction with CO.

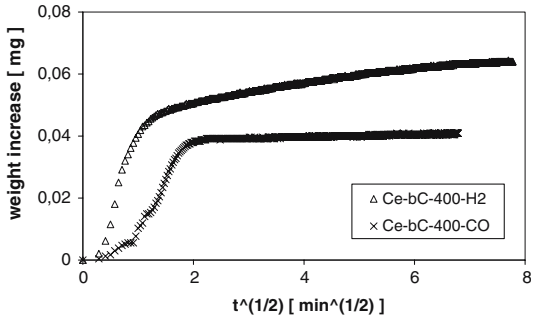

Figure 3. Weight increase during N_2O titration (10 vol% N_2O/Ar, 75 °C, flow rate 80 ml/min) normalized with the total weight loss upon reduction on Ce-bC-400 as a function of square root of time. Pre-reduction was performed either with 7 vol% H_2 or with CO in argon (260 °C, 2 h, heating rate 2 K/min, flow rate 80 ml/min). The reduced sample was cooled in the reduction gas prior to N_2O titration.

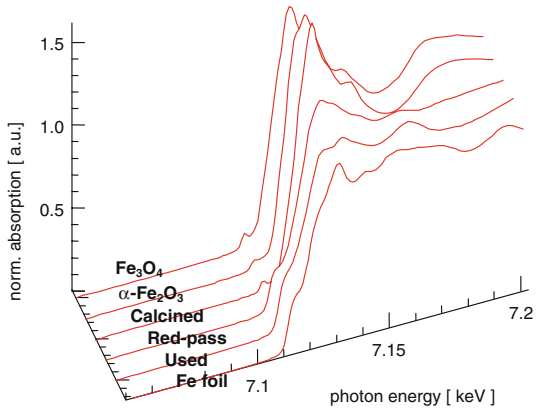

Figure 5. XAS spectra of the Ni–Fe mixed oxide catalyst recorded at the Fe K-edge. XANES profiles are shown for the calcined, reduced-(O_2) passivated and the used samples together with the reference compounds α-Fe_2O_3, Fe_3O_4 and Fe-foil.

3.2. Nickel–iron catalyst

The Ni–Fe catalyst was investigated by XAS, in particular in the XANES region. By recording data at both the Ni K-edge and the Fe K-edge, the oxidation state of both metals can be determined. Figures 4 and 5 show the XAS spectra of Ni and Fe, respectively, for the calcined and reduced-passivated samples and for the sample used in the synthesis of CNFs. The spectra of NiO, a Ni foil, α-Fe_2O_3, Fe_3O_4 and a Fe foil are used as references.

Figure 6 shows a least squares fit of a linear combination of the XANES spectra of model compounds, reconstructing the profile of a catalyst sample. NiO and Ni foil are combined in order to model the XANES profile of the reduced-passivated Ni–Fe catalyst at the Ni K-edge. According to this fit, 70% of the Ni atoms in the sample are in the metallic state after O_2-passivation while 30% are re-oxidized to NiO. Table 2 contains the phase composition for the three Ni–Fe catalyst samples recorded at both the Ni and the Fe K-edge. The Ni sample profiles are modelled with two reference materials, since Ni(0) and Ni(2+) are the most common oxidation states of nickel. The Fe sample profiles are reconstructed with three reference materials, since Fe(0) under low partial pressure of oxygen first oxidizes to Fe_3O_4 (= $FeO{\cdot}Fe_2O_3$) and then further to Fe_2O_3 [2].

The XANES analysis of the Ni K-egde of the sample used for CNF production shows that essentially all Ni is preserved as Ni(0). Reduced Ni particles encapsulated in carbon nanofibers (see also [15]) thus preserve their metallic state also upon exposure to air. The encapsulation in carbon is better than passivation by O_2, where about 30% of the Ni atoms are re-oxidized to NiO, assuming that both H_2 reduction and reduction under CNF production conditions result in complete conversion of NiO to metallic Ni prior to oxygen exposure. About 80% of the iron atoms in the CNF-encapsulated sample retain the metallic state, as compared to about 60% with oxygen passivation. The remaining 20 or 40%

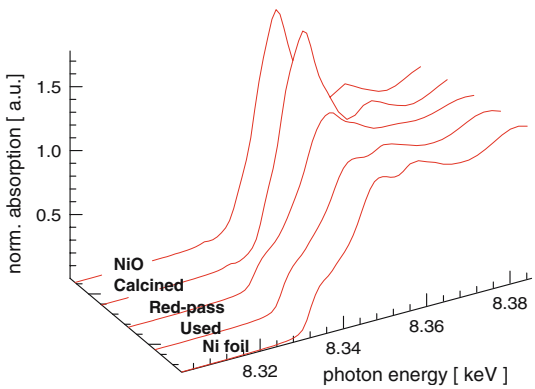

Figure 4. XAS spectra of the Ni–Fe mixed oxide catalyst recorded at the Ni K-edge. XANES profiles are shown for the calcined, reduced-(O_2) passivated and used samples together with the reference compounds NiO and Ni-foil.

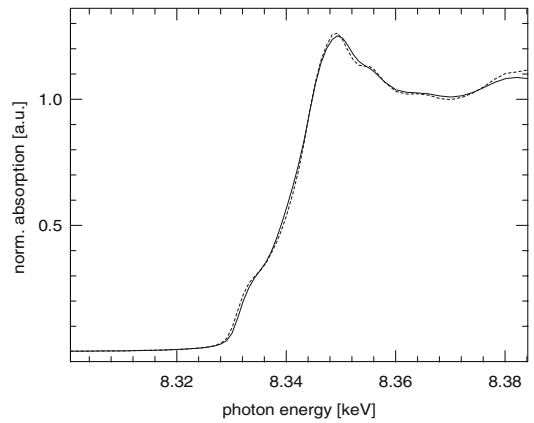

Figure 6. Least-squares fit (dashed line) of the XANES spectra (solid line) of the reduced-(O_2) passivated Ni-containing sample at the Ni K-edge. The fit is produced by linear combination of the XANES spectra of the model components NiO and Ni-foil using a Levenberg–Margquardt least squares algorithm in the WINXAS software.

Table 2
Phase composition of the Ni–Fe catalyst sample (passivated with O_2), determined by a linear combination of XANES data of the reference materials at the Ni and the Fe K-edge applying a least-squares fitting algorithm in the software package WINXAS

Ni K-edge:			
Sample	Ni metal (%)	NiO (%)	
Calcined	7	93	
Reduced-passivated	70	30	
Used	98	2	
Fe K-edge:			
Sample	Fe metal (%)	α-Fe_2O_3 (%)	Fe_3O_4 (%)
Calcined	0	65	35
Reduced-passivated	57	39	4
Used	82	10	8

are present as a mixture of Fe_3O_4 and Fe_2O_3. The 20% non-metallic Fe atoms in the CNF-encapsulated sample have either been re-oxidized under air exposure or they represent a fraction of iron atoms not reducible under the given pre-reduction and CNF-production conditions (see also [45]). Correspondingly, the oxide fraction in the O_2-passivated sample may also contain the non-reducible part, in addition to the oxide formed under passivation conditions.

3.3. Cobalt catalyst

Figure 7 shows XRD spectra of the calcined Co/SiO_2 catalyst, as well as after reduction and passivation with oxygen. The XRD profile recorded after passivation with N_2O is identical to the one after passivation with oxygen, and is hence not included in the figure. The nine main peaks in the spectrum for the calcined sample can be assigned to Co_3O_4. In addition, there are two broad peaks between 10 and 30 ° stemming from the silica support. For the passivated sample, the characteristic Co_3O_4 peaks have vanished and the apparent peaks can be assigned to CoO and metallic cobalt. The broad peak at 36–37° is assigned mainly to CoO, but it cannot be excluded that Co_3O_4 contributes to the right shoulder of this peak. The broad shoulder between 46–54° can be assigned to different metallic cobalt phases.

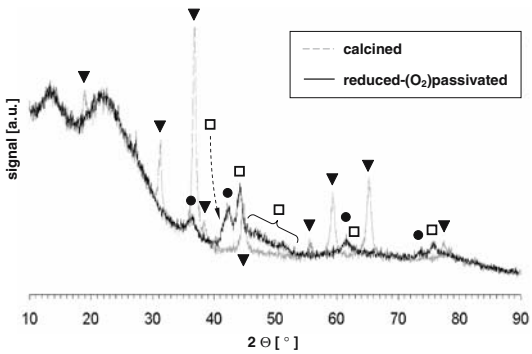

Figure 7. XRD spectra of Co/SiO_2 for calcined and reduced-(O_2) passivated samples. The symbols refer to different crystalline phases: ▼ = Co_3O_4, ● = CoO, □ = Co. The profile of the reduced-(N_2O) passivated sample is identical to the spectra of the O_2-passivated sample and is therefore not shown in the figure.

4. Discussion

From dispersion measurements of copper catalysts [20,22,27,38,42], it is well-known that the re-oxidation of the reduced metal with O_2 or N_2O is not limited to the surface, but also reaches sub-surface layers. As a consequence, these measurements are either conducted at low temperatures (for O_2 [20]) or the contribution of the bulk oxidation is taken into account applying a diffusion model (for N_2O [38,42]).

4.1. Thermodynamics and kinetics

Standard reaction enthalpies for the oxidation of Cu, Ni, Fe and Co by O_2 and N_2O are shown in table 3. They are estimated from the standard enthalpies of formation of the compounds participating in the reactions, based on bulk data. The oxidation processes investigated in this study are limited to a few nanometers into the bulk of the metals. Thus, pure bulk data may not be accurate for quantifying the energies involved in these reactions, but can be used for qualitative comparisons.

The values for the O_2 oxidation are calculated for 1 mol O_2 and not for 1 mol O, which one might prefer when comparing with the values for N_2O oxidation. We prefer the O_2-based enthalpies because each time an O_2 molecule reacts with the metal, two oxygen atoms are involved simultaneously in the oxidation reaction releasing the double amount of energy of one oxygen atom. Thus, we prefer to compare N_2O and O_2 based on the amount of energy these two molecules contain in total.

The following trends can be deduced from the thermodynamic data in table 3:

Table 3
Thermodynamics of the metal oxidation by O_2 and N_2O, based on the standard enthalpies of formation for the bulk metals

	Standard reaction enthalpy (kJ/mol)[a]	
	N_2O (per mole N_2O)	O_2 (per mole O_2)
$Cu \rightarrow Cu_2O$	−250	−337
$Ni \rightarrow NiO$	−318	−472
$Fe \rightarrow Fe_2O_3$	−354	−543
$Fe \rightarrow Fe_3O_4$	−358	−408
$Co \rightarrow CoO$	−316	−468
$Co \rightarrow Co_3O_4$	−303	−442

[a] From standard enthalpies of formation: N_2O: 82 kJ/mol, Cu_2O: −168 kJ/mol, NiO: −236 kJ/mol, Fe_2O_3: −815 kJ/mol, Fe_3O_4: −1103 kJ/mol, CoO: −234 kJ/mol, Co_3O_4: −885 kJ/mol. Per definition, the standard enthalpy of O_2 is zero. The enthalpy of the metals is set to zero as well, although small enthalpies of formation (absolute values < 7 kJ/mol) are tabulated for some metallic phases of Ni, Fe and Co ([46] and references therein).

- The oxidation reactions are all exothermic. This is reflected in the well-known pyrophoric behaviour of reduced transition metal catalysts in contact with air.
- The oxidation reaction with N_2O is less exothermic than with O_2, i.e., during the consumption of one O_2 molecule more energy is released as per N_2O molecule.
- For N_2O, the energy release during oxidation of the different metals increases in the following order: Cu < (Ni, Co) < Fe. The same order is obtained for oxidation with O_2, if Fe_2O_3 is the main phase formed. The stability of the metallic phase decreases in the same order.
- Copper may be considered the thermodynamically most stable among the four metals. Ni and Co behave relatively similar, while for Fe the energy released depends strongly on the type of oxide formed. These thermodynamic properties are to some extent responsible for Ni, Co and Fe being more difficult to reduce than Cu, as reflected in the typical reduction temperatures for these metals.

Apart from thermodynamics, there are also kinetic effects to be considered. According to Pernicone *et al.* [20], temperature is a main parameter influencing the extent of bulk oxidation using O_2. Because the passivation process is a non-catalytic gas–solid type reaction [47], the passivation rate and thus the extent of bulk oxidation depends on the diffusion rate in the solid material with the diffusion coefficient being a function of temperature. The kinetic rate constant of the oxidation reaction itself is also enhanced by increasing temperature, although we assume that the diffusion process is the rate-limiting step during bulk oxidation with O_2. In principle, this is also the case for passivation with N_2O [27,38,42].

Via the interrelation between temperature and passivation kinetics, the thermodynamics affects the kinetics of the process. Because of the exothermic nature of the oxidation reactions, energy is released and the local temperature increases. The energy release may thus enhance the diffusion rate and increase the extent of bulk oxidation. According to this, the extent of bulk oxidation should be higher for passivation with O_2 than with N_2O, not taking into account the effect of different oxidation kinetics for O_2 and N_2O. Bartley *et al.* [27] identify local temperature increases as a significant cause for bulk oxidation of Cu in dispersion measurements with O_2 and N_2O. They stress the need for low oxidant concentrations, large sample amounts and characterization setups with efficient heat dissipation, resulting in a more controlled release of the heat of the oxidation reactions.

4.2. Copper catalysts

The higher extent of bulk oxidation with O_2 as compared to N_2O (table 1) we assume does not only stem from the effect discussed above, especially since the passivation with N_2O is conducted at higher temperatures and higher gas concentration than the passivation with O_2. Other factors could be the somewhat higher sample amount used for the O_2 passivation (because of requirements for the subsequent XRD analysis) and the different reaction rate constants for N_2O and O_2, with N_2O enabling a more controlled passivation. This might also be reflected in that Cu dispersion measurements conducted with O_2 are performed at very low temperatures while the N_2O method can be performed at ambient temperatures and even up to 90 °C.

The question remains whether the thin oxide layer produced with N_2O is sufficient to protect the metallic copper core against further bulk oxidation in air. The observed dependence of the passivation degree on the size of the copper particles (Chapter 3.1, and similar discussion about higher reactivity of small metal particles in [27] and references therein) implies that a certain, stable passivation layer thickness is required. Furthermore, the similar XRD profiles for the Co catalyst sample passivated in O_2 and N_2O (figure 7) point in the same direction. Bartley *et al.* [27] report that they could not prevent some continued re-oxidation of copper after applying a N_2O passivation procedure that resulted in a thin oxide layer around the metallic copper core. If N_2O initially creates a passivation layer thinner than O_2 does, yet not stable enough to survive in ambient air atmosphere, further bulk oxidation leads to a thicker, metastable passivation layer of similar thickness as created by O_2 passivation. Hence, even though N_2O does not lead to a stable passivation layer, it can be used in a first passivation step to grow an oxide layer that will slow down further re-oxidation with O_2 and prevent local temperature increase, thereby keeping the final thickness of the passivation layer at a minimum.

Moreover, in analogy with electrochemical processes [48], it is possible that Cu(2+) might be formed in ambient atmosphere at the surface of the passivation layer by adsorbing oxygen and/or H_2O (from air moisture) leading to formation of $Cu(OH)_2$ and/or CuO at the surface [2].

4.3. Nickel–iron catalyst

The Ni(2+) detected by XAS in the Ni–Fe–Al sample is identified as NiO. This oxidation state could also be assigned to a Ni–Al spinel structure known to form at high calcination temperatures [49]. However, Ni incorporated in such a structure is less reducible, and would not be reduced under the conditions applied here [15]. The spinel structure is detectable in XRD if formed to a significant extent [49], but was not found for the Ni–Fe–Al sample calcined at 480 °C [15]. Ni K-edge data of the CNF-encapsulated sample also show that almost 100% of Ni remains in the metallic state after CNF production at 600 °C. Consequently, the sample probably does not contain XRD amorphous Ni–Al-spinel, since basically

all Ni can be reduced. The reduced-passivated sample is treated up to the same temperature. It is thus likely that the detected Ni(2+) stems from NiO formed during passivation.

The reliability of the phase composition data obtained by the least-squares fitting procedure depends on a reasonable choice of reference materials, i.e., fitting of the experimental curve might still be possible even when using unreasonable model compounds. The quality of the recorded spectra is also vital to the fitting procedure. According to the XANES fit, the calcined sample contains around 7% Ni metal. It appears unlikely that Ni particles oxidized in air at 480 °C contains significant amounts of metallic nickel. The XANES curves of the calcined sample and the NiO reference (not shown) display similar profiles. The difference between these curves is a certain deviation in the high energy part of the recorded spectra, believed to emerge from measurement (e.g., thickness effects) and/or data treatment rather than being related to the material itself. As a consequence, the 7% of Ni metal obtained for the calcined sample should be treated as an error, indicating the accuracy limit of the linear combination approach for this system. The values presented in table 2 should thus be viewed as average values with an accuracy not better than ± 5% composition percentage. For comparison, the standard deviations given by Overbury *et al.* [50] represent a qualitative assessment of the accuracy limit of a linear combination of XANES data.

Yu *et al.* [15] performed an EXAFS analysis for the Ni–Fe sample investigated here. In their structural model, the extent of re-oxidation during passivation was estimated to about 26% for Ni and 35% for Fe, when comparing the co-ordination numbers (N) of the oxygen shells of the calcined and reduced-passivated samples (*Iron:* first Fe–O shell N = 1.1 and second Fe–O shell N = 3.5 for the calcined sample, first Fe–O shell N = 0.3 and second Fe–O shell N = 1.3 for the passivated sample; *Nickel:* first Ni–O shell N = 5.4 for the calcined sample, first Ni–O shell N = 1.4 for the passivated sample). These values are in the same range as the values in table 2.

The thermodynamic prediction that Ni is more stable than Fe (when forming Fe_2O_3) can be supported by the XAS data. The extent of bulk oxidation upon O_2-passivation of Cu in the TGA (table 1) is, however, slightly higher than the one obtained for Ni with XAS. The stability of the metal phase might depend on particle size and co-additives in the catalytic material, as can be seen from the comparison of the three copper catalysts, thus making interrelationships more complex than comprised in a mere discussion of thermodynamic trends. As previously mentioned, a practical aspect with regard to hot spots is for example the choice of equipment used during passivation [27]. The Cu catalysts were passivated in a TGA sample pan with small dimensions, i.e., each sample was concentrated in a small volume implying a certain risk for local temperature increase. In contrast, the Ni–Fe catalyst was passivated in a conventional calcination reactor with large dimensions, the sample being distributed over a larger area compared with the TGA pan and a lower risk for hot spots.

4.4. Cobalt catalyst

XRD was used to qualitatively identify the main phases present in the samples after passivation (figure 7). The oxidation of cobalt is similar to the oxidation of nickel from an energetic point of view (table 3). Not taking into account kinetics, it should therefore be possible to passivate cobalt in the same manner as nickel. The XRD profile of the O_2-passivated sample in figure 7 confirms the presence of metallic cobalt encapsulated in a CoO shell. The reduction of Co_3O_4 to metallic cobalt proceeds via CoO [3,4]. Under mild conditions (low temperature and low oxygen concentration) the re-oxidation may only proceed to the intermediate CoO (in analogy with the behaviour of copper), since CoO is stable under certain conditions [2]. Yet, the existence of a Co_3O_4 phase (a mixture of $Co^{(2+)}O$ and $Co^{(3+)}{}_2O_3$ [2]) in the passivated samples cannot be ruled out. The CoO detected by XRD may originate either from the passivation process or from CoO not reduced during the reduction step. Cobalt oxide supported on silica is easily reduced from Co_3O_4 to CoO independent of particle size, morphology and support properties, but the reduction of CoO to Co is more difficult and depends on particle size and support properties [4]. According to Storsæter *et al.* [34], about two-thirds of the silica-supported cobalt is reducible (determined by oxygen titration) upon reduction in hydrogen at 350 °C for 16 h. About one-third remains unreduced even upon a subsequent TPR up to 900 °C, and might be assigned to cobalt silicate or cobalt oxide encapsulated in silica [4,21]. An *in situ* XAS analysis suggested that the degree of reduction is around 80% which is somewhat higher than determined by oxygen titration [3].

4.5. Encapsulation in carbon

Encapsulation of reduced metals in carbon appears to be an efficient way to protect metallic phases against re-oxidation in air. The encapsulation in CNF is, however, not a generally applicable technique, since it applies only to catalysts active for carbon formation. Jacobs *et al.* [17] used the solidified, paraffinic Fischer–Tropsch wax product as an encapsulation matrix to preserve the reduced state of cobalt in a used Fischer–Tropsch catalyst. A more generally applicable encapsulation procedure mentioned in literature is the deposition of polyethylene [11–13] or 1-butene [14] films at the catalyst surface, in analogy with the protection of bulk metals against electrochemical corrosion by coating with polymer films.

4.6. Methods combining carbon and oxide formation

The treatment in a mixture of CO and H_2 to form a layer of carbonaceous species on the catalyst surface was reported to be superior to passivation with oxygen for reduced cobalt particles [32]. However, a measured temperature increase upon air exposure (lower than for passivation with oxygen [32]) can be interpreted as an indication for the formation of an oxide layer. The conditioning of reduced catalysts with CO_2 at elevated temperature (e.g., 200 °C) has been applied to the passivation of Ni–Cr/Al_2O_3 steam-reforming-methanation catalysts [51]. Furthermore, the XPS and XRD data of Cu-based [52] and Cu–Co-based [53] catalysts that had been exposed to CO/CO_2-containing gas mixtures during the synthesis of alcohols are relevant also to passivation. Metallic copper and Cu_2O were identified by XRD for a Cu–ZnO–Al_2O_3 catalyst after use in methanol synthesis [52]. However, we suggest to assign the corresponding XPS spectra to Cu(1+) rather than to Cu(0) or a mixture of both species, in agreement with literature [48,54] and the well-known instability of Cu(0) in oxidizing atmosphere (i.e., air). For the Cu–Co-based catalysts used in the synthesis of higher alcohols, metallic Co as well as oxidized Co species were identified by XPS [53].

Passivation strategies that involve CO and/or CO_2 without the formation of significant amounts of coke or wax around the metal particles may comprise both formation of carbonaceous species and an oxide layer (at the latest when exposed to air), depending on the conditions used and the metal to be passivated. Deactivation studies carried out on ceria-supported precious metal catalysts indicate that CO and CO_2 can adsorb at catalyst surfaces during reactor shutdown forming stable surface carbonates [55]. Vissokov [29] claims that the rate of oxidation could be lowered, hence the passivation improved, by the ability of certain metals to form surface complexes (e.g., metal carbonyl), but oxidation could not be prevented completely under the conditions used. These findings are in line with the results shown in figure 3. Pre-treatment with CO instead of H_2 resulted in a slower oxidation kinetics and a lower oxygen uptake during N_2O titration, which might be related to the formation of carbonaceous surface species limiting the access of N_2O. Such methods may therefore be considered intermediate between encapsulation with carbon and formation of a protective oxide layer, with the carbonaceous surface layer suppressing the extent of bulk oxidation.

5. Conclusions

Studies of reduced metal catalysts based on Cu, Ni, Fe and Co show that the result of passivation procedures should be monitored, in order to quantify the extent of bulk oxidation. Heat released during exothermic oxidation reactions appear to be a critical parameter, since the local temperature and hence bulk diffusion and the final extent of bulk oxidation may be increased. Furthermore, the (oxidic) passivation layer requires a certain thickness in order to be stable and prevent further bulk oxidation in ambient air atmosphere.

Passivation of reduced catalysts is not an ideal strategy for characterization of reduced systems that are unstable in air. *In situ* measurements are prefered, but passivated samples can be used to some extent, e.g., for estimating particle size with XRD [20,33], keeping in mind the limited relevance and accuracy of data derived from this approach. The use of passivated samples for a detailed X-ray line broadening analysis, in correlation with catalytic activity, distinguishing between particle size and strain effects is questionable and requires evaluation by a parallel *in situ* approach. Through the passivation procedure, strain may be introduced into the crystal lattice by the oxidation of the outer metal layers. Possible morphological changes depending on the reduction/oxidation potential of the surrounding atmosphere may also complicate the interpretation of the characterization results. Finally, the discussion of active reaction sites based on the characterization of passivated samples is disputable.

Encapsulation of reduced metal particles by a protective layer of carbon is found to efficiently protect Ni particles. For certain catalysts, CNF encapsulation could be preferred instead of passivation by a protective oxide layer. Provided that the carbon layer is impermeable to oxygen when exposed to air, the reduced metal particles may be preserved in their metallic, hence active, state. Possible morphological changes as a result of a change in the reduction/oxidation potential of the surrounding atmosphere should be of less concern than for passivation with oxygen. However, the particle morphology might be affected by the CNF growth process [56].

With this paper, we want to call more attention to the passivation procedure, its effect and limited usability as sample treatment prior to characterization.

Acknowledgments

This work was supported by the Research Council of Norway through Grant No. 140022/V30 (RENERGI). Statoil ASA through the Gas Technology Center NTNU-SINTEF is also acknowledged for their support. We gratefully acknowledge the project team at the Swiss-Norwegian Beam Lines (SNBL) at the ESRF for their assistance. Elin Nilsen (Department of Materials Technology, NTNU) and Egil Haanæs (Department of Chemical Engineering, NTNU) are gratefully acknowledged for their assistance with the XRD devices and the TGA, respectively. Hilde Meland and Cathrine Bræin Nilsen (Department of Chemical Engineering, NTNU)

are gratefully acknowledged for preparing the copper catalysts.

References

[1] J.A. Rodriguez, J.Y. Kim, J.C. Hanson, M. Perez and A.I. Frenkel, Catal. Lett. 85 (2003) 247.
[2] A.F. Hollemann and E. Wiberg, *Lehrbuch der Anorganischen Chemie* 101 ed.(Walter de Gruyter, Berlin, 1995).
[3] Ø. Borg, M. Rønning, S. Storsæter, W. van Beek, A. Holmen, Appl. Catal. A (accepted).
[4] D.G. Castner, P.R. Watson and I.Y. Chan, J. Phys. Chem. 94 (1990) 819.
[5] R.B. Greegor and F.W. Lytle, J. Catal. 63 (1980) 476.
[6] J.D. Grunwaldt, A.M. Molenbroek, N.Y. Topsøe, H. Topsøe and B.S. Clausen, J. Catal. 194 (2000) 452.
[7] M.M. Günter, B. Bems, R. Schlögl and T. Ressler, J. Synch. Rad. 8 (2001) 619.
[8] P.L. Hansen, J.B. Wagner, S. Helveg, J.R. Rostrup-Nielsen, B.S. Clausen and H. Topsøe, Science 295 (2002) 2053.
[9] W.P.A. Jansen, J. Beckers, J.C. van den Heuvel, A.W. Denier van den Gon, A. Bliek and H.H. Brongersma, J. Catal. 210 (2002) 229.
[10] M. Rønning, T. Gjervan, R. Prestvik, D.G. Nicholson and A. Holmen, J. Catal. 204 (2001) 292.
[11] M.P. Kapoor, Y. Ichihashi, K. Kuraoka, W.-J. Shen and Y. Matsumura, Catal. Lett. 88 (2003) 83.
[12] W.-J. Shen, Y. Ichihashi and Y. Matsumura, Catal. Lett. 79 (2002) 125.
[13] W.-J. Shen, Y. Ichihashi and Y. Matsumura, Catal. Lett. 83 (2002) 33.
[14] S. Zhao and R.J. Gorte, Catal. Lett. 92 (2004) 75.
[15] (a) Z. Yu, T. Vrålstad, M. Rønning, E. Ochoa-Fernández, D. Chen, A. Holmen, Manuscripts, part 1 and 2, in preparation; (b) Z. Yu, PhD Thesis, (Norwegian University of Science and Technology, Trondheim, 2005).
[16] M.L. Toebes, J.H. Bitter, A.J. van Dillen and K.P. de Jong, Catal. Today 76 (2002) 33.
[17] G. Jacobs, T.K. Das, P.M. Patterson, J. Li, L. Sanchez and B.H. Davis, Appl. Catal. A 247 (2003) 335.
[18] T. Huizinga, J. van Grondelle and R. Prins, Appl. Catal. 10 (1984) 199.
[19] E. Crezee, P.J. Kooyman, J. Kiersch, W.G. Sloof, G. Mul, F. Kapteijn and J.A. Moulijn, Catal. Lett. 90 (2003) 181.
[20] N. Pernicone, T. Fantinel, C. Baldan, P. Riello and F. Pinna, Appl. Catal. A 240 (2003) 199.
[21] R. Riva, H. Miessner, R. Vitali and G. Del Piero, Appl. Catal. A 196 (2000) 111.
[22] J. Ma, C. Park, N.M. Rodriguez and R.T.K. Baker, J. Phys. Chem. B 105 (2001) 11994.
[23] R.M. Rioux and M.A. Vannice, J. Catal. 216 (2003) 362.
[24] E.K. Poels and D.S. Brands, Appl. Catal. A 191 (2000) 83.
[25] H. Wilmer, M. Kurtz, V. Klementiev, O.P. Tkachenko, W. Grünert, O. Hinrichsen, A. Birkner, S. Rabe, K. Merz, M. Driess, C. Wöll and M. Muhler, Phys. Chem. Chem. Phys. 5 (2003) 4736.
[26] X. Huang, L. Ma and M.S. Wainwright, Appl. Catal. A 257 (2004) 235.
[27] G.J.J. Bartley, R. Burch and R.J. Chappell, Appl. Catal. 43 (1988) 91.
[28] A.M. Alekseev, A.V. Mikhailova, V.S. Beskov, G.S. Shitikova, B.N. Kuznetsov, Khimicheskaya Promyshlennost (russ.) 2 (1995) 99.
[29] G.P. Vissokov, J. Mater. Sci. 28 (1993) 6457.
[30] V.V. Dergachev, A.V. Krylova, SU Patent 1,625,520 (1991).
[31] A.V. Krylova, N.V. Nefedova, L.D. Kuznetsov, P.D. Rabina, G.A. Ustimenko, T.L. Koroleva, P.T. Mikhailovich, N.S. Torocheshnikov, SU Patent 1,250,319 (1986).
[32] S. Hammache, J.G. Goodwin and R. Oukaci, Catal. Today 71 (2002) 361.
[33] M. Rønning, F. Huber, H. Meland, H. Venvik, D. Chen and A. Holmen, Catal. Today 100 (2005) 249.
[34] (a) S. Storsæter, Ø. Borg, E.A. Blekkan, A. Holmen, J. Catal. 231 (2005) 405; (b) S. Storsæter, B. Tøtdal, J.C. Walmsley, B.S. Tanem, A. Holmen, J. Catal. 236 (2005) 139.
[35] A. Dandekar, R.T.K. Baker and M.A. Vannice, J. Catal. 183 (1999) 131.
[36] G.C. Chinchen, C.M. Hay, M.D. Vandervell and K.C. Waugh, J. Catal. 103 (1987) 79.
[37] G. Jacobs, E. Chenu, P.M. Patterson, L. Williams, D. Sparks, G. Thomas and B.H. Davis, Appl. Catal. A 258 (2004) 203.
[38] S. Sato, R. Takahashi, T. Sodesawa, K. Yuma and Y. Obata, J. Catal. 196 (2000) 195.
[39] V.R. Palkar, P. Ayyub, S. Chattopadhyay and M. Multani, Phys. Rev. B 53 (1996) 2167.
[40] J. Lemaître, P.G. Menon and F. Delannay, , Pages 299– in: *Characterization of Heterogeneous Catalysts*, F. Delannay (eds.), (Marcel Dekker, New York, 1984) pp. 299–.
[41] T. Ressler, J. Synch. Rad. 5 (2004) 118.
[42] J.R. Jensen, T. Johannessen and H. Livbjerg, Appl. Catal. A 266 (2004) 117.
[43] B.S. Clausen and J.K. Nørskov, Top. Catal. 10 (2000) 221.
[44] I. Kvande, D. Chen, M. Rønning, H.J. Venvik and A. Holmen, Catal. Today 100 (2005) 391.
[45] J.W. Niemantsverdriet, J.A.C. van Kaam, C.F.J. Flipse and A.M. van der Kraan, J. Catal. 96 (1985) 58.
[46] P.C. Hayes, *Process Principles in Minerals and Materials Production* (Hayes Publishing Co., Brisbane, 2003).
[47] O. Levenspiel, *Chemical Reaction Engineering* 3 ed.(John Wiley & Sons, New York, 1999).
[48] U. Collisi and H.-H. Strehblow, J. Electroanal. Chem. 284 (1990) 385.
[49] K.M. Lee and W.Y. Lee, Catal. Lett. 83 (2002) 65.
[50] S.H. Overbury, D.R. Huntley, D.R. Mullins and G.N. Glavee, Catal. Lett. 51 (1998) 133.
[51] I.J. Kitchener, EP Patent 89,761 (1983).
[52] X. Dong, H.-B. Zhang, G.-D. Lin, Y.-Z. Yuan and K.R. Tsai, Catal. Lett. 85 (2003) 237.
[53] H.-B. Zhang, X. Dong, G.-D. Lin, X.-L. Liang and H.-Y. Li, Chem. Commun. 40 (2005) 5094.
[54] (a) J.P. Espinos, J. Morales, A. Barranco, A. Caballero, J.P. Holgado, A.R. Gonzalez-Elipe, J. Phys. Chem. B 106 (2002) 6921; (b) J. Morales, J.P. Espinos, A. Caballero, A.R. Gonzalez-Elipe, J.A. Mejias, J. Phys. Chem. B 109 (2005) 7758.
[55] X. Liu, W. Ruettinger, X. Xu and R. Farrauto, Appl. Catal. B 56 (2005) 69.
[56] Z. Yu, D. Chen, B. Tøtdal and A. Holmen, Catal. Today 100 (2005) 261.